Nonlocal quantum macroscopic superposition in a high-thermal low-purity state

Mark E. Brezinski* and Bin Liu

Center for Optical Coherence Tomography and Optical Physics, Department of Orthopedic Surgery, Brigham and Women's Hospital, 75 Francis Street, Boston, Massachusetts 02115, USA and Harvard Medical School, 25 Shattuck Street, Boston, Massachusetts 02115, USA

(Received 13 December 2007; revised manuscript received 15 October 2008; published 16 December 2008)

Quantum state exchange between light and matter is an important ingredient for future quantum information networks as well as other applications. Photons are the fastest and simplest carriers of information for transmission but in general, it is difficult to localize and store photons, so usually one prefers choosing matter as quantum memory elements. Macroscopic superposition and nonlocal quantum interactions have received considerable interest for this purpose over recent years in fields ranging from quantum computers to cryptography, in addition to providing major insights into physical laws. However, these experiments are generally performed either with equipment or under conditions that are unrealistic for practical applications. Ideally, the two can be combined using conventional equipment and conditions to generate a "quantum teleportation"-like state, particularly with a very small amount of purity existing in an overall highly mixed thermal state (relatively low decoherence at high temperatures). In this study we used an experimental design to demonstrate these principles. We performed optical coherence tomography (OCT) using a thermal source at room temperatures of a specifically designed target in the sample arm. Here, position uncertainty (i.e., dispersion) was induced in the reference arm. In the sample arm (target) we placed two glass plates separated by a different medium while altering position uncertainty in the reference arm. This resulted in a chirped signal between the glass plate reflective surfaces in the combined interferogram. The chirping frequency, as measured by the fast Fourier transform (FFT), varies with the medium between the plates, which is a nonclassical phenomenon. These results are statistically significant and occur from a superposition between the glass surface and the medium with increasing position uncertainty, a true quantum-mechanical phenomenon produced by photon pressure from two-photon interference. The differences in chirping frequency with medium disappears when second-order correlations are removed by dual balanced detection, confirming the proposed mechanism. We demonstrated that increasing position uncertainty at one site leads to position uncertainty (quantum position probability amplitude) nonlocally via second-order correlations (two-photon probability amplitude) from a low coherence thermal source (low purity, high local entropy). The implications, first, are that the phenomenon cannot be explained through classical mechanisms but can be explained within the context of quantum mechanics, particularly relevant to the second-order correlations where controversy exists. More specifically, we provide the theoretical framework that these results indicate a nonlocal macroscopic superposition is occurring through a two-photon probability amplitude-induced increase in the target position probability amplitude uncertainty. In addition, as the experiments were performed with a classical source at room temperature, it supports both the quantum-mechanical properties of second-order correlations and that macroscopic superposition is obtainable in a target not in a single coherent state (mixed state). Future work will focus on generalizing the observations outside the current experimental design and creating embodiments that allow practical application of the phenomenon.

DOI: 10.1103/PhysRevA.78.063824 PACS number(s): 42.50.Ct, 42.50.Dv, 42.50.Ar

INTRODUCTION

Macroscopic superposition and nonlocality, particularly through the two-photon probability amplitude, have generated considerable interest in recent years due to their relevance in such diverse areas as telecommunication, cryptography, computers, metrology, and medicine. Macroscopic superposition, the production of a so-called "Schrödinger cat" state, has now been achieved with such diverse objects as atoms [1], molecules [2], current states [3], mirrors [4,5], and amplitude-dispersed photons [6]. However, the majority of macroscopic superposition experiments are performed with relatively complex system designs and well below room temperature. This limits their use for practical applications. Ideally, the two can be combined using conventional equipment and conditions to generate a "quantum teleportation"-like state, particularly with a very small amount of purity and high entropy existing in an overall [7] very highly mixed thermal state of the target.

Nonlocal quantum phenomenon, particularly entangled states and/or thermal two-photon probability amplitudes, have also generated considerable interest over recent years stemming from such seminal work as the Einstein, Podolsky, Rosen (EPR) thought experiment and Bell's inequality to current studies on second-order correlations [8–11]. This has ranged from quantum imaging to quantum computers and cryptography [12–17]. However, the majority of entanglement experiments are performed with low intensity, complex

*Corresponding author: Mark E. Brezinski; FAX: (617) 732-6705; mebrezin@mit.edu

quantum sources such as those that operate through spontaneous parametric down conversion (SPDC) [12,18]. However, recently the potential of thermal sources, operating through second-order correlations, has been examined for producing nonlocal effects [19–22]. While the effects seen in some studies using second-order correlations, particularly those in the field of ghost imaging, have been disputed as classical versus quantum mechanical in nature; others have clear quantum origins [10,11,23,24]. Examples where quantum effects are noted with a thermal source include resonant interaction with two-level atoms, entanglement of an arbitrarily large mixed state with a single qubit in a pure state, and the transfer of a qubit entanglement to the entanglement between thermal and vacuum states [19,25–27]. Furthermore, evidence supports that nonlocal interactions can occur with mixed states even in the setting of high entropy, which will be demonstrated in the experiment [28,29].

As stated, many areas of science and engineering would benefit from combining macroscopic superposition and nonlocality, such as the correction of quantum computer errors [22,30,31]. Photons are the fastest and simplest carriers of information for transmission but, in general, it is difficult to localize and store photons, so usually one prefers choosing matter as quantum memory or storage elements. With the combination, quantum information can be transferred completely, through superposition and nonlocality, potentially with no decoherence, from one object to another [30–34]. The ability to perform quantum teleportation-like behavior, particularly at room temperature with a thermal source, could be a powerful advance for a wide range of fields in which quantum information transfer would be useful. In this work, we examine this phenomenon using a specifically designed target and an optical coherence tomography (OCT) system with precise dispersion control (phase and envelope) of the probability amplitude.

OCT is based on low coherence interferometry, and is currently being used for a wide range of applications [35–37]. OCT is analogous to ultrasound, measuring the back reflection of infrared light rather than sound. Most systems utilize a Michelson interferometer and a low coherent thermal source. The technique allows micron scale ranging in real time. In addition, the system chosen here had a grating-based delay line that allowed manipulation of the phase and envelope of the probability amplitude.

In this study, we examine nonlocal position uncertainty changes (increased quantum position probability amplitude) transfer using second-order correlations via a two-photon probability amplitude. To achieve this, dispersion (and therefore position uncertainty) is induced with the reference arm chosen for phase and envelope control. The sample arm target (optimized for this experiment) consists of two reflecting surfaces, separated by a medium of different refractive indices, which are imaged as dispersion is varied in the reference arm. Changing the degree of dispersion in the reference arm results in varying chirping in the interferogram. The spatial frequency of the chirping is measured by performing a fast Fourier transform (FFT) on the interferogram. Classically, the spatial frequency of chirping between the two targets in the sample arm would be unaffected by the medium present in between. Comparisons of data obtained from either a single detector or a dual balanced detector OCT system, the latter of which was designed to reduce second-order correlations, is examined to determine mechanisms behind results that deviate from classical predictions. The implications of these results are dealt with in the Discussion.

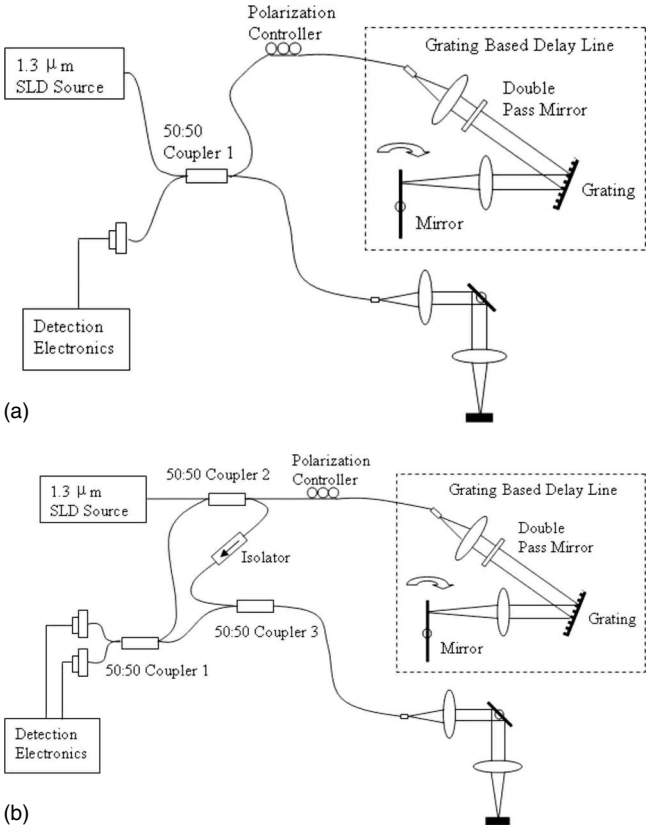

FIG. 1. Diagrams of two configurations of the fiber-based OCT systems: (a) the single-detector OCT setup and (b) the dual-balanced-detector OCT setup. The latter is used to remove second-order correlations.

METHODS

In Fig. 1, we demonstrate the two configurations of the fiber-based OCT systems used for interferogram detection. Figure 1(a) depicts the schematics of the single-detector OCT setup, and Fig. 1(b) shows the dual-balanced-detector OCT setup. In either setup, a wideband light source (AFC, Toronto, Canada) is used with a central wavelength of ~1310 nm and ~60 nm full-width-half-maximum (FWHM) bandwidth. Vacuum fluctuations enter through the exit port of the beam splitter, the potential significance of which is discussed below [25]. For dual balanced detection, which is designed to substantially reduce second-order correlations, all the return beams recombine at both exit ports of the coupler 1 to construct two channels of identical interferograms but 180° out of phase [38].

As stated, we induced position uncertainty in the reference arm through a grating-based delay line, which is shown in Fig. 2 [39]. Here, the collimated incident light beam is projected to a diffractive grating with an entrance angle θ_i.

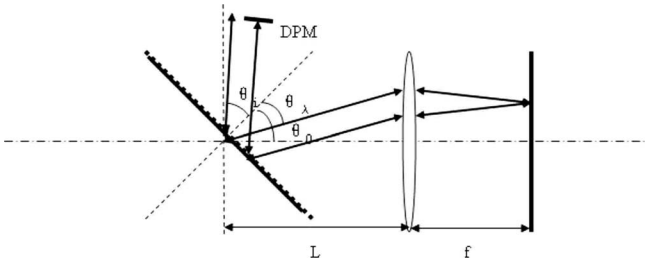

FIG. 2. Schematics of a grating-based optical delay line.

Due to the broadband nature of the light source, each spectral component of the beam with wavelength λ is dispersed spatially with diffractive angle θ_λ. Light is then projected to a mirror through a lens and reflected to the grating. As the mirror is located in the focal plane of the lens, the different wavelength components exit in the reverse direction of the incident light with a wavelength-dependent linear phase ramp. The tilting angle of grating's normal with respect to the optical axis is represented as θ_0. The distance between the incident point of the grating and the lens is L. The focal length of the lens is f. A second mirror, labeled DPM for double pass mirror, is employed in the system as a "double pass" optical delay line. This optical delay line is based on Fourier transform pulse-shaping techniques. By tilting the mirror, different linear phase ramps are introduced. Because of the Fourier relationship, a linear phase ramp in the frequency domain results in an optical group delay in the time domain. This delay line is able to scan several millimeters with repetition rates of several kHz and allows independent control of phase and group delay.

For such a setup, the equivalent group velocity dispersion (GVD) is formulated as [40]

$$\mathrm{GVD} = -2m^2\lambda_0^3(L-f)/\pi c^2 d^2 \cos\theta_0, \tag{1}$$

where d is the grating spacing and m is the diffraction order used in the delay line. If the grating is placed at a point other than the focal point of the lens, in other words, $(L-f)$ is nonzero, a GVD in the reference arm is induced and is variant with L (i.e., increased uncertainty).

The sample arm target was specifically chosen to study the physical principles relevant to this manuscript, as will become apparent. The sample arm configuration is shown in Fig. 3. The thickness of the glass slides, which are in a wedge shape, are large (>1 mm) compared to that of the gap (15–40 μm optical distance). Therefore, only the two gap

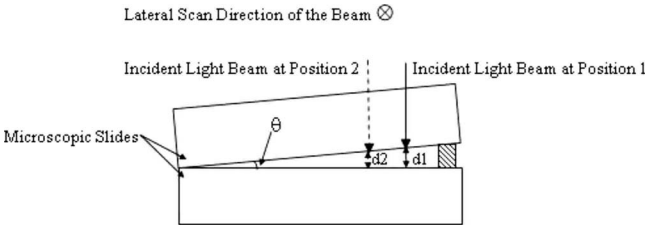

FIG. 3. Configuration scheme of the sample arm, in which the optical-distance light travels as well as the medium type is controllable.

interfaces show up as reflections. Along the paper plane, the thickness of the gap varies continuously as the existence of the angle θ. This angle is 0.6° to maintain a 1000:1 horizontal to vertical ratio. In other words, if the stage translates about 1 mm horizontally the distance of the gap changes 1 μm. With tiny angle θ, the incident light beam is nearly perpendicular to the interfaces. The glass slides are on a three-dimensional movable stage with 0.1 μm resolution.

We obtain measurements of a medium of three different group refractive indices, air (1.00), water (1.34), and oil (1.68) in the gap region by an investigator blinded to the hypothesis. The optical group refractive indices are confirmed by previously described methods [41]. *A* scans are obtained at optical distances of 15, 20, 30, and 40 μm for all three mediums. The 15 μm point is chosen rather than 10 μm as the theoretical and measured resolution of the source is 12.2 μm in air. At each gap distance, we perform displacement of the mirror in the reference arm from 0 to 3 cm at increments of 0.5 cm. A 1 cm displacement corresponds to a theoretical classical point spread function (PSF) of 66.7 um while 2 cm displacement would be 133.4 μm [40,42]. As the mirror is displaced, each peak in the *A* scan interferogram widens until chirping occurs. The FFT is measured for each A-scan and plots are made of spatial frequency against displacement. The same experiment is done with both single-detector and dual-detector OCT system setups to study the possible difference in susceptibility to the medium. A total of six trials at all combinations were performed, all on separate days.

Unfortunately, the literature tends to focus on dispersion of the envelope and neglects variations of k in the time or spatial domain. The equation that describes the classically dispersed interference signal (both envelope and phase) is therefore derived in Appendix A as follows:

$$I(\Delta z) \approx I_R + I_S + \frac{I_0}{2} p_R p_S \cos[2\pi n(k_0) k_0 \Delta z + C] \times \exp\left[-\frac{4\ln 2 n^2(k_0)\Delta z^2}{\delta_l'^2}\right]\Bigg\}. \tag{2}$$

The most critical term here is the C, which classically is a constant and contains $2\pi n'(k_0) z_R$. Other terms are defined in Appendix A. A linear phase variation is assumed here for simplicity but other frequency variations are equally valid. This represents the frequency variation within the envelope. It may be seen here and in the Appendix that the nonlocal macroscopic superposition between the medium and reflecting surface cannot be explained classically if it is dependent on the medium between reflectors.

Dr. Liu, who performed all experiments, was blinded to the hypothesis. Averages and standard deviations were taken of all six trials at each dispersion displacement with each medium. Data from each medium is compared using ANOVA with parametric methods assuming $p<0.05$ is significant.

RESULTS

In Fig. 4, we show example *A* scans and FFTs. The top is a separation of the two glass plates by 30 μm where there is

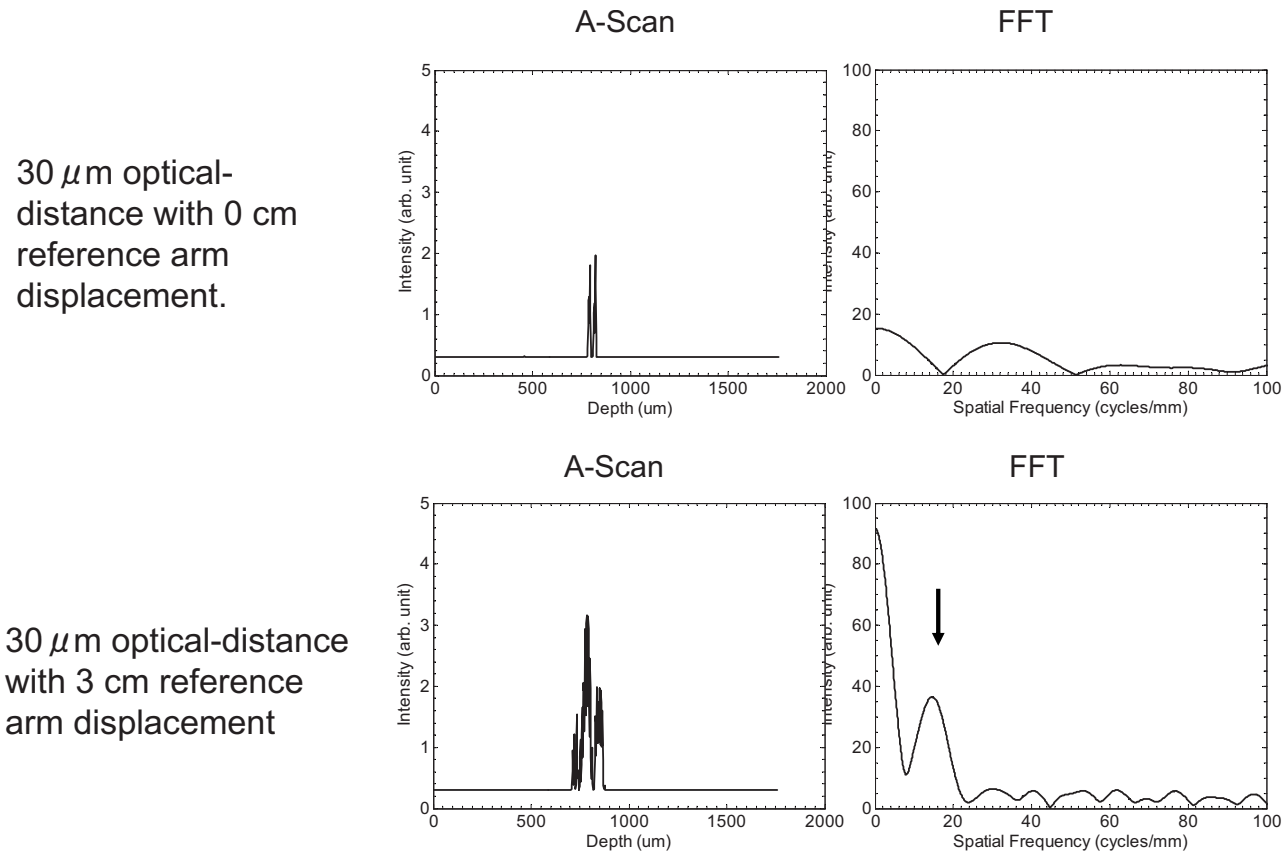

FIG. 4. Example *A* scans and FFTs of the sample with different dispersions in the reference arm. The top is a separation of the two glass plates by 30 μm where there is no displacement of the grating in the reference arm (0 dispersion). It can be seen that only a diffuse peak from the separation of the two slides is noted in the FFT. In the lower figures, the glass plates are again separated by 30 μm, but the grating in the reference arm is displaced 3 cm. It can be seen in the *A* scan that the signal is now chirped, with its spatial frequency identified by the arrow in the FFT.

no displacement of the mirror in the reference arm (0 dispersion). It is demonstrated that no well-defined peak is noted in the FFT from the separation of the two slides. In the lower figures, the glass plates are again separated by 30 μm, but the grating in the reference arm is displaced 3 cm. It can be seen in the *A* scan that the signal is now chirped, with its spatial frequency identified by the arrow in the FFT.

In Fig. 5(a), we perform plots of the reference arm displacement versus FFT with lipid being compared to air in the sample arm. The left column is single-detector measurements while the right sample arm target is performed with a dual detector OCT system. Individual graphs represent different gap widths imaged through (as marked). It should be noted that, in the single-detector measurements, statistically significant differences exist between lipid and water in the region where chirping initiation is occurring (1–2 cm displacement). At points with no chirping (<1 cm displacement), no difference exists between the air and oil as expected. Similarly, with displacements greater than 2.5 cm, which corresponds to a classical PSF greater than 165 μm, the vast majority of the returning sample arm signal is from the glass slide (2 mm in diameter versus a maximum 40 μm gap width) so no difference is noted. When dual-balanced detection is performed, in contrast, no statistically significant difference among mediums under any condition is noted. Figure 5(b) demonstrates a similar comparison between water and air, with a lower refractive index mismatch than the lipid and air. Although a trend exists similar to that for lipid, only one point is statistically significant. Again, no effect is noted when dual-balanced detection was utilized.

Gap sizes of 40 μm or greater were not examined because more than one spatial frequency was noted in the FFT (arrows). This is seen in Fig. 6 where the arrows delineate two relatively large spatial frequencies in the FFT, in addition to multiple smaller ones. These greater gap sizes are not amenable to the single-frequency approach in Fig. 5, nor are they necessary to test the hypothesis.

DISCUSSION

This study demonstrates that macroscopic superposition, at room temperature (mixed target state) using a conventional thermal source (low purity), can be induced through nonlocal manipulation of the two-photon probability amplitude (second-order correlations). The design of this experiment, particularly target and delay line configuration, demonstrates several observations of substantial significance that are theoretically modeled in the discussion below. First, controversy exists as to whether certain effects of second-order correlations are classical or quantum mechanical in origin, in

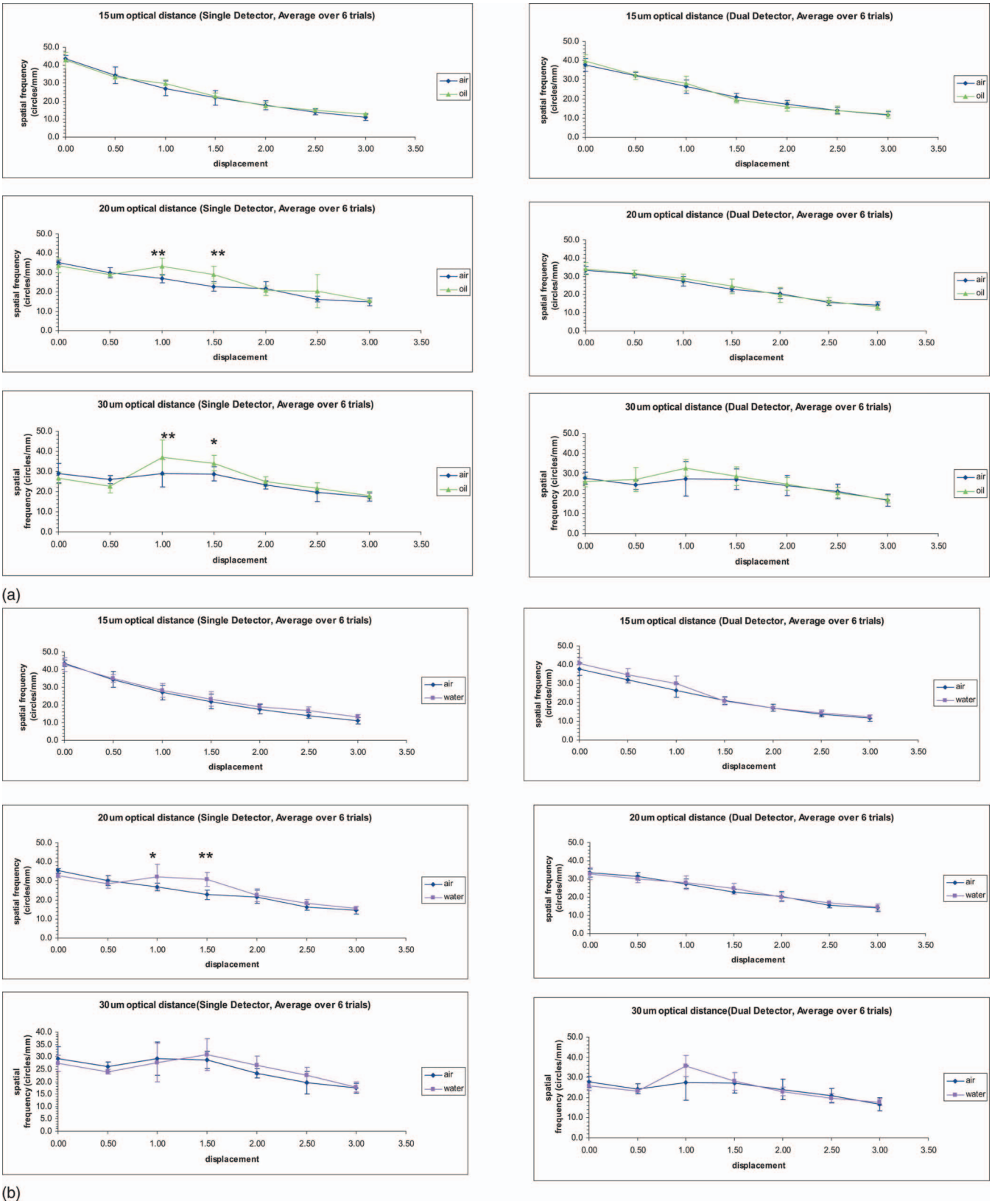

FIG. 5. (Color) Plots of peak spatial frequency versus reference arm displacement, with 15 μm, 20 μm and 30 μm optical-distance separation, respectively. (a) Plots for lipid and (b) plots for water, being compared to air in the sample arm. The left column is single-detector measurements while the right is performed with dual-detector measurements. Classically, the curves should be identical. In the figures * is $p<0.05$, ** is $p<0.01$, and *** is $p=0.05$.

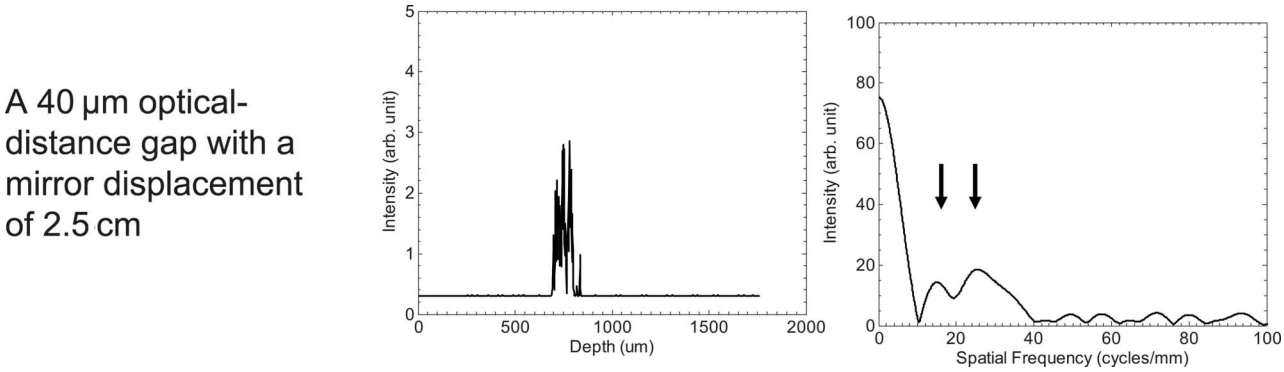

FIG. 6. The *A* scan and its FFT of a 40 μm optical-distance gap with the reference arm displacement of 2.5 cm. Multiple peaks are noted, making it unusable for evaluation in Fig. 5.

spite of several recent theoretical papers convincingly supporting the latter [10,11,23,24]. With the design of the experimental setup in this paper, the results are easily explainable within the framework of quantum mechanics. However, classical optics fails to provide an adequate explanation. Second, the nonlocal macroscopic superposition was produced utilizing a thermal source, both supporting the nonclassical properties of the two-photon probability amplitude and that these observations are achievable at low purity. Third, the experiments were done at room temperature, requiring no "exotic" experimental setup and demonstrating the target does not need to be in a single coherent state. Fourth, the fact that quantum phenomenon could be demonstrated at room temperature demonstrates a relative stability from decoherence. Finally, the end result was a system where photons were used to nonlocally "transmit" quantum-mechanical properties while the storage was achievable in macroscopic superposition of the target, the advantages of which are discussed in the Introduction.

Macroscopic quantum interference between surfaces has been previously described with OCT, albeit using a SPDC source among other differences. A group from Boston University using SPDC photons have noted a peak between two silica plates, which they referred to as quantum cross interference [43,44]. This peak can be positive or negative, depending on the experimental conditions. When a dispersive element was placed in the sample arm, they noted broadening of this peak, but not the peaks representing the silica surface. There are at least four important distinctions between their work and the data presented in this paper. First, dispersion is produced in our work nonlocally by manipulation in the reference arm rather than a dispersive element in the sample arm. Second, superposition is observed with a thermal source (i.e., conventional OCT system) rather than through SPDC. Third, target design, along with use of a thermal source and grating-based delay line, was such that it allowed the demonstration that the second-order correlations exhibited effects that could not be explained classically. Fourth, interface broadening was not seen in their experimental design (related to the use of a SPDC source).

The experimental setup in this paper in the near field is similar to recent "ghost imaging" experiments as opposed to earlier Hanbury Brown Twiss (HBT) experiments that are performed in the far field. A low coherence interferometer (OCT) was used with a precision dispersion control delay line in the reference arm while the target in the sample arm was two silica plates separated by a medium of varying refractive index. As dispersion was induced in the reference arm, broadening of the two silica interfaces occurred in the *A* scans with chirping in the interferogram. The induction of chirping in and of itself, or the varying of chirping frequency, can be described by classical optics and is particularly sensitive to the phase asymmetry, in addition to envelope broadening, which develops in the autocorrelation function, the relevance of which is discussed below. However, the chirping frequency was sensitive to the medium between the two silica plates in the sample arm where no dispersive element was present. The implications of this observation are that nonlocal induction of macroscopic superposition and increased uncertainty in the position probability amplitude has occurred. The mechanism allowing the nonlocal nature of the results is dispersion of the two-photon probability amplitude. This mechanism is supported by the fact that the phenomenon could be completely eliminated with dual-balanced detection, which removes second-order correlation (Appendix B).

The effects of first-order correlations seen in this paper have been previously described in detail and are the basis of OCT imaging, which relies predominantly on classical physics. However, modeling of the dispersion phase asymmetry from the grating-based delay line, which is described in Appendix A, has not been previously described. While it can be completely described with classical optics, its derivation was necessary for discussing two-photon probability amplitude dispersion, a quantum-mechanical entity with no classical analog. The phase asymmetry is modeled most prominently in the *C* term, which here is taken as a linear phase ramp of the form $2\pi n'(k_0)z_R$ as well as containing the full width at half maximum of the broadened envelope δ_l'. Therefore, other than the derivation in Appendix A and the reference arm dispersion, the physical principles behind low coherence interferomtery with first-order correlations are not discussed in detail.

The quantum-mechanical basis for observations seen in these experiments are initially modeled separately in parts of the interferometer with descriptions of grating-based line dispersion, the induction of increased position probability amplitude by photon pressure from second-order correlations,

the nonlocal properties of the two-photon probability amplitude, and theory behind dual-balanced detection. These "components" are brought together in a total coherent superposition. Other approaches, that could have been taken to model these observations include a Gaussian-state framework (phase insensitive autocorrelation function, phase sensitive cross correlation function, and phase insensitive cross correlation function with proper versus improper P representations) or a many-particle Bose gas (although the lack of vacuum fluctuations may need to be accounted for) analogous to a set of quantized harmonic oscillators. Neither of these approaches are undertaken here, though parts of the latter are used below.

Target design is critical to the experiment. As stated, the target consists of two silica plates separated by three different mediums. In the final theoretical derivation below, this target is going to viewed as a thermally mixed collection of quantum-mechanical harmonic oscillators. However, to build this framework, we will leverage modeling done with some recent work studying macroscopic superposition with a fixed mirror and movable mirror (oscillating) and a single photon that forms a coherent state between them [4,5,45–49]. The coupling is achieved through photon pressure and it seems that leveraging the modeling off this heavily studied area is the most straightforward approach. However, the experiments are generally done with relatively complex experimental designs, single photons, and temperatures well below room temperature, which is not the case in the experiments described in this paper. The use of extremely low temperatures increases the viability of representing the oscillator mirror as a single harmonic oscillatory, but the current work and theoretical work of others shows that superposition and system coherence is achievable with a target or field in a mixed thermal state. Nevertheless, the use of this model initially gives a relatively straightforward representation for understanding how photon pressure can result in position uncertainty in the harmonic oscillator. When this model is extended to the approach used in this experiment, the mirror as the oscillator will be replaced by a collection of harmonic oscillators constituting the target, and the single photon will be replaced by two photons of varying frequency composition and phase. As the two photons become dispersed via manipulations in the reference arm, position uncertainty increases through alterations in the photon pressure spatial distribution and phase.

In using the two mirrors and single photon described in the previous paragraph, we are primarily interested in generating the coupling constant G, the baseline position uncertainty of the mirror σ, and κ the maximum displacement of the mirrors center of mass in units of the size of ground-state uncertainty. The radiation pressure is the force per unit area and is given by $hk/2\pi$. As with the previous publications using the two mirrors and the photon, the distinction between momentum, pseudomomentum, and wave momentum in the material is ignored as it does not add to understanding of the model but for those interested, the topic has been treated in great detail elsewhere [50]. The mirror and later the quantum harmonic oscillators will increase or decrease energy levels in units of phonons (bosons). The most commonly used Hamiltonian (here with phase modification) describing the coherent state of the two mirrors and photon is

$$\hat{H}_k = \hbar\omega_k\left(a_A^\dagger a_A e^{i\theta_k} + \frac{1}{2}\right) + \hbar\omega_m\left(b^\dagger b + \frac{1}{2}\right) - \hbar G a_A^\dagger a_A e^{ia\theta_k}(b + b^\dagger). \tag{3}$$

The first term of the Hamiltonian represents the free photon where ω_k is the photon angular frequency and $a^\dagger a$ represents the creation or annihilation operators of the photon in normal ordering. The term $e^{i\theta_k}$ has been added here to improve understanding of the physics, which for a single photon is a trivial term, but when we move to a broadband dispersed two-photon probability amplitude becomes important in understanding observed physical phenomenon (placed here for illustrative purposes). It is added here to emphasize the phase sensitivity but will be moved into the coupling term later in the derivation. The second term represents the state of the mirror without interaction with the photon where ω_M (for mirror of mass M), $b^\dagger b$ are the creation or annihilation operators for the phonons, and $1/2$ represents the fact the lowest energy level is nonzero. The third term couples the oscillatory mirror and photon where G is the coupling term given by

$$G = \frac{\omega_k \sigma_0}{L}, \tag{4}$$

and σ_0 is the baseline mirror or oscillator uncertainty, which equals (de Broglie wavelength)

$$\sigma_0 = \left(\frac{\hbar}{2m\omega_m}\right)^{1/2}. \tag{5}$$

The normalized state of the mirror $|\alpha_i\rangle$ has an amplitude of

$$|\alpha_i\rangle = \kappa(1 - e^{i\omega_m t}) = \left(\frac{\hbar\omega_k^2}{2m\omega_m L}\right)(1 - e^{i\omega_m t}). \tag{6}$$

Again the parameter κ quantifies the displacement or uncertainty of the mirror in units of the ground-state uncertainty of the mirror to that perturbed by the photon(s) and is given by

$$\kappa = \frac{G}{\omega_m} = \frac{\omega_k \sigma}{\omega_m L} = \frac{\omega_k}{\omega_m L}\left(\frac{\hbar}{2m\omega_m}\right)^{1/2} = \left(\frac{\hbar\omega_k^2}{2m\omega_m L}\right)^{1/2}. \tag{7}$$

It links the unperturbed mirror uncertainty to the perturbed uncertainty induced by the photon. The critical point here is that, as k increases with either increasing the bandwidth or the phase varies among different k values, the amplitude of the state of the mirror increases (position uncertainty amplitude). Then κ and G become

$$\kappa = \int\left(\frac{\hbar\omega_k^2 e^{i\theta_k}}{2\omega_m L}\right)d\omega, \quad G = \int\frac{\omega_k \sigma_0 e^{i\theta_k}}{L}d\omega. \tag{8}$$

The Hamiltonian now becomes

$$\hat{H}_k = \hbar\omega_k\left(a_A^\dagger a_A e^{i\theta_k} + \frac{1}{2}\right) + \hbar\omega_m\left(b^\dagger b + \frac{1}{2}\right) - \hbar G a_A^\dagger a_A (b + b^\dagger). \tag{9}$$

In the previous discussion representative of derivations from several publications, the coherent state superposition was done such that the mirror was treated as a single harmonic oscillator [45–49]. Experiments were performed at extremely low temperatures to reduce the number of excitation states (Boltzmann distribution). However, the mirror, or in this case of the current experiment, the entire target can be treated as consisting of many oscillators at different energy levels without loss of utility of the model. In other words, a mixed thermal state can be in a macroscopic superposition and it is not required that the macroscopic object be in a single coherent condition. So, extending this to the target in the experiment, both the glass and medium are viewed as consisting of harmonic oscillators with varying ω_M and M (reduced mass), as well as varying "spring constants." At baseline, without two-photon stimulation, the uncertainties are assumed to be small and the medium and silica boundaries sharp. However, with interaction with the broadband two-photon probability amplitude, the broad number of oscillator frequencies and varying relative phase relationships increases position uncertainty. Again, to simplify the physical representation without loss of validity of the model, for descriptive purposes, we are going to take advantage of the fact that a 1300 nm median wavelength was used in this experiment. Generalizing, this is the wavelength region for absorption of many strong molecular vibration modes so that for the point of illustration, the classic oscillating weight on a spring with different phases, reduced masses, and oscillatory frequencies is useful. Put another way, the photon-phonon interaction will be considered exclusively to occur in molecular vibrational states without loss of viability of the model. In addition, rather than a single photon, the target is exposed to broadband low coherence light with varying dispersion (the separate treatment of first- and second-order correlations will be dealt with later).

Now focusing our attention on the grating-based delay line, we and others have discussed the underlying physical principles, which allow control of phase and group delay [35]. These are not discussed here but have been described elsewhere in detail. The equation that describes dispersion production in the delay line is given in the methods section without derivation [Eq. (1)]. The dispersion is controlled by the distance between the lens and grating. This dispersion analysis has been extended in this paper (Appendix A) to include carrier phase asymmetry that is necessary for describing chirping phenomenon. So, when $L=f$, no dispersion occurs in the Gaussian spectrum. However, as this distance is altered, dispersion is induced in the backreflected reference arm light (and as we will see, the two-photon wave function).

In modeling so far, we saw at the target in the sample arm where photon pressure resulted in changes in position probability amplitude (a quantum-mechanical effect) and in the reference arm the induction of dispersion via a grating-based delay line. The latter was treated classically because for the purposes of this experiment, we are only interested in frequency-dependent phase shifts, broadening of the probability amplitude, and asymmetry in the carrier frequency within the envelope, which can be directly applied to the development of the two-photon probability amplitude. The target and photon in the grating-based delay line will be brought together through the second-order correlations, specifically a field of two-photon probability amplitudes of varying k and phase values. Evidence for the role of the two-photon or nonlocal effects come from the results of the experiment indicating a measurable, statistically significant superposition occurring between the medium and glass in the sample arm as a function of dispersion induction in the reference arm. This phenomenon could be completely eliminated by removal of second-order correlations with dual-balanced detection. Both the removal with dual-balanced detection and the nonlocal nature indicate the effect is not due to first-order correlations and cannot be explained classically.

First-order correlations are a coherent effect of the electric field. Until recently, it has been strongly argued that second-order correlations were classical statistical correlations. But the second-order correlation is a coherent effect of the two-photon probability amplitude. In modeling the two-photon probability amplitude, for simplicity, the photon is going to be destroyed at the target and mirror (absorption). The back-reflection to the detector is not critical to the analysis except a subsequent discussion of the dual-balanced detection. This approach makes understanding the principles vastly easier without loss of generality. From the quantum theory of photodetection, where the mirror and target represent the photodetector, the second-order correlation function is given by

$$G^{(2)}(t_1,r_1;t_2,r_2) = \mathrm{Tr}[\hat{\rho}E_1^{(-)}(t_1,r_1)E_2^{(-)}(t_2,r_2)E_2^{(+)}(t_2,r_2)E_1^{(+)} \times(t_1,r_1)]. \tag{10}$$

Here Tr is the trace and $\hat{\rho}$ is the density operator. The two non-Hermitian operators $\hat{E}^{(+)}$ and $\hat{E}^{(-)}$ are the positive and negative frequency components of the electric-field operator. The electric-field operator can be expressed more explicitly as

$$\hat{E}^{(+)}(r,t) = [\hat{E}^{(-)}(r,t)]^{\dagger} = i\int_0^{+\infty}\left(\frac{\hbar\omega_k}{2\varepsilon_0\nu}\right)^{1/2}\bar{e}_k\hat{a}_k \times\exp[i(nk\cdot r-\omega_k t)]dk. \tag{11}$$

Here n is the composite refractive index of the superposition, $\bar{e}_k$ is the polarization vector, v is the volume, and $\hat{a}_k$ is the annihilation operator. Equation (10) is modeling the second-order correlations as an incoherent statistical mixture of two photons with equal probability of having any momentum q and q' [10]. Then the density operator of the second-order correlations can be written as

$$\hat{\rho}\propto\sum_q\sum_{q'}|1_q1_{q'}\rangle\langle 1_q1_{q'}|. \tag{12}$$

The spatial portion of the second-order correlation function can be written using Eqs. (10) and (12) as (where x_1 and x_2 are the positions of the mirror and target) [10]

$$G^{(2)}(x_1;x_2) = \sum_{q,q'} \langle 1_q 1_{q'} | E_1^{(-)}(x_1) E_2^{(-)}(x_2) E_2^{(+)}(x_2) E_1^{(+)}(x_1) | 1_q 1_{q'} \rangle$$
$$= \sum_{q,q'} |\langle 0 | E_2^{(+)}(x_2) E_1^{(+)}(x_1) | 1_q 1_{q'} \rangle|^2. \quad (13)$$

The electric-field operator is now rewritten as

$$\vec{E}_j^{(+)}(x_j) \propto \sum_q f_j(x_j;q)\hat{a}(q). \quad (14)$$

Here $j=1$ or 2 represent the sample arm or reference arm. Here the annihilation operator corresponds to a given mode and $f(x_j;q)$ is a spatial distribution function. The f_2 term contains the dispersion variation. Now substituting the field operators into Eq. (13), the second-order correlation function becomes

$$G^{(2)}(x_1;x_2) \propto \sum_{q,q'} |f_2(x_2;q)f_1(x_1;q') + f_2(x_2;q')f_1(x_1;q)|^2. \quad (15)$$

The interference here is not due to the superposition of electromagnetic fields as in classical optics at a focal point in space time. It is due to a superposition of the terms on the right side of the summation. Equation (15), which models the results of this experiment, has no classical parallel and is the basis of the nonlocality. Note that term containing the dispersion, f_2, is inseparable from the f_1 term. This equation can be rewritten in terms of first-order correlation functions (though it is a second-order effect) as follows:

$$G^{(2)}(x_1;x_2) \propto \sum_q |f_1(x_1;q)|^2 \sum_{q'} |f_2(x_2;q')|^2 + \left| \sum_q f_1^*(x_1;q) f_2(x_2;q) \right|^2 = G_{11}^{(1)}(x_1) G_{22}^{(1)}(x_2) + |G_{12}^{(1)}(x_1;x_2)|^2. \quad (16)$$

The events are occurring at two independent locations even though they are expressed in terms of first-order correlations. An intriguing aspect of Eq. (16) is that the second term, generated from thermal radiation, represents a coherent superposition. This is consistent with arguments raised earlier in the discussion that a coherent field is not necessary for developing coherent superposition.

How the effect is removed by dual-balanced detection involves two different concepts. The first and most obvious is that the superposition is caused should be detected by the second-order correlations as no difference occurs among the medium when second-order correlations are removed from detection (i.e., first-order correlations alone show no difference among the medium). The quantum theory of dual-balanced detection is described in Appendix B. But the second point, which is more subtle but intriguing, is that the superposition is not directly detected by the first-order correlations as the effect is completely removed with dual-balanced detection. Even though the superposition is being caused by the second-order correlations, why are the first-order correlations not detecting or ranging a superposition (caused by two-photon probability amplitude) even when dual-balanced detection is used (i.e., why is the effect completely removed)? If the superposition was caused by the two-photon but the uncertain target position ranged by both the first- and second-order correlations, then the effect would not be completely removed by dual-balanced detection. While photon statistics can be used to describe this phenomenon, simply viewing the bunched photons as intensity correlation while viewing the first-order correlations as field correlations is sufficient. The bunched photons again are intensity correlations and are removed with dual-balanced detection for reasons described in Appendix B. The first-order correlations as a correlation in the electrical field are predominately not removed by dual-balanced detection. Therefore, it can be envisioned that the superposition is maximum when bunching is maximal (highest photon pressure) and that these high uncertainty backreflected photons therefore occur at relatively high concentrations at this time of maximal bunching. Then, there is a high correlation between the concentration of photons which apply the photon pressure and the backreflected signal leading to detection of increased uncertainty.

How does the two-photon effect and photon pressure effect the chirping frequency of the OCT interferogram between two reflections? Before directly answering this question, some discussion as to why chirping was studied is warranted. Phase sensitive OCT, using the phase component of the autocorrelation function in addition to the envelope, theoretically has a superior sensitivity than measuring the envelope alone. However, in practice, OCT system designs sensitive to phase have been susceptible to artifacts such as movement and angle changes [51–53]. Chirping is a direct result of how phase overlap is occurring. This is the reason this specific target was designed. Analyzing a chirped signal between two reflectors at a fixed distance represents a distinct way from previous approaches for indirectly using phase information, which avoids artifacts such as motion and changing surface angle. This is supported by the extremely low variability in measurements, made weeks apart, seen in Figs. 5(a) and 5(b), particularly those using dual-balanced detection.

Second-order correlations show up in two ways in OCT imaging. First, some groups have used entangled photons as described above, generated from an SPDC source, to produce OCT images with very high resolutions, albeit at low photon counts and long acquisition rates [43,44]. Second, it is known that second-order correlations alter the traditional OCT interferogram and are treated as a noise source, which is why dual-balanced detection is now used in most conven-

tional OCT systems. It is clear that both first-and second-order correlations contribute to the interferogram; second-order correlations can be used to improve sample characterization or serve as a noise source. In this experiment, the ability of the two-photon probability amplitude to alter position probability amplitudes leads to varying overlap between the two reflecting surfaces. Since this results in an actual superposition between the medium and reflecting surfaces, and not just dispersion broadening occurring from poor ranging by a broadened reference arm PSF, the medium in-between the reflecting surfaces alters chirping frequency through second-order correlations, a nonclassical phenomenon.

Similarities and differences in the properties of entangled photons (SDPC) and second-order correlations (thermal sources) are being studied extensively, including in the fields of quantum and classical ghost imaging, interaction between the mixed states and two-level atoms, and exchanges between mixed states, the vacuum state and qubit [12,22]. Entangled two-photon systems are generally characterized by two peculiar properties: (1) coherent superposition of two-photon amplitudes and (2) correlation in both momentum and position variables. Making a distinction between the two-photon probability amplitude and an entangled state is not a focus of this paper. But the two-photon probability amplitude in this experiment has quantum-mechanical properties, which cannot be derived classically, particularly nonlocality. One point should be raised for consideration regarding vacuum fluctuations entering the exit port of the interferometer and whether this alters the quantum effects of second-order correlations. This work is somewhat related to work that has similar theoretical implications including two-level atom resonant interaction following entanglement, arbitrarily large mixed states with small qubit in a pure state, and the transfer of a qubit entanglement to the entanglement between thermal and vacuum states [19,25–27]. For example, with the resonant two-level atoms, this groups work shows that a cavity field can evolve to a macroscopic superposition through interaction with a resonant two-level atom even if it is initially in a thermal state [19]. Returning to the vacuum fluctuations at the exit port, in the classic HBT experiments, the target is before the beam splitter, but here, like in ghost imaging studies, the target is in the near field. That means second-order correlations interact with vacuum fluctuations in the beam splitter. There remains the possibility that this interaction increases the ability of second-order correlations to demonstrate nonlocal phenomenon [25]. Whether this is an actual phenomenon that alters the properties of second-order correlations and contributes to the quantum controversy remains the source of future investigation. In particular, in the work examining the interaction of vacuum fluctuation at the beam splitter (which is distal to the target), the entanglement property can be seen in the similarity between Eq. (9) and Eq. (11) [25]. From this study, two important factors are necessary. The first is that the source is operating at relatively high intensity (i.e., not in photon counting range) with high photon excess noise. This alleviates any controversy when working in the photon counting range. High entropy is not an issue as discussed above. The second is that the target, in contrast to a Brown-Twiss interferometer, is after the beam splitter, allowing the intense thermal beam to interact with the vacuum fluctuations entering the exit port. Both of these are met with the current experiment.

For completeness, it can be stated that the effect is not due to classical dispersion of the medium in the sample arm for several reasons [Eq. (2)]. First, dispersion is negligible compared to that in the reference in the region where the effect was prevalent (Fig. 5). For water at 1.3 μm, $k''=-0.100+/-0.002$ fs^2 μm. Second, the effect disappears when second-order correlations were eliminated through dual-balance detection. If the effect had occurred with first-order coherence rather than second-order, it would have violated the widely held belief that these correlations cannot be used to distinguish classical from quantum effects [20,54]. This would have required reevaluation of the conclusions. Third, the two reflectors broadened symmetrically rather than the deeper peak broadening more than the superficial peak. Finally, the observations cannot be attributed to differences in reflectivity as again it disappears with dual-balanced detection.

The major limitation of the study is the large width of the glass slides (greater than 1 mm), which limits the reference arm displacements over which the effect can be noted. At reference arm displacements greater than 2 cm, no effect is noted. At this level of displacement, the vast majority of the classical PSF extends into the glass slide and only a small portion represents an overlap of the gap containing the medium. Therefore, no difference among the medium exists or is expected. While the current experimental design does test the hypothesis successfully, the width of the targets would ideally be on the order of the coherence length to allow differences to extend beyond 2 cm displacement. Similarly, use of a source with higher excess noise will also likely increase differences between different mediums. Furthermore, some data suggest that the use of broader bandwidths may improve delineation among the medium [55].

As with the demonstration of many quantum-mechanical phenomena, such as the demonstration of sub-Poisson light or photon bunching, the results in these experiments are far from dramatic in terms of the magnitude of change [56–61]. However, the implications of these results nonetheless have powerful implications. The subtle result is that chirping frequency between two glass plates varies, in a statistically significant manner, with the medium between the reflecting surface and that this effect is completely eliminated when dual-balanced detection is implemented. The implications, first, are that the phenomenon cannot be explained through classical mechanisms but can be explained within the context of quantum mechanics. More specifically, we provide the theoretical framework that these results indicate a nonlocal macroscopic superposition is occurring through a two-photon probability amplitude-induced increase in target position probability amplitude uncertainty. In addition, as the experiments were performed with a classical source at room temperature, it supports both the quantum-mechanical properties of second-order correlations and that macroscopic superposition is obtainable in a target not in a single coherent state (high entropy and low purity). The relevance of these observations is to such diverse areas as telecommunication, cryptography, computers (quantum bit error corrections), metrol-

ogy, medicine, and even testing modeling of collapse. Future work will focus on generalizing the observations outside the current experimental design and creating embodiments that allow practical application of the phenomenon.

ACKNOWLEDGMENTS

This research is sponsored by the National Institutes of Health, Contracts No. R01-AR44812 (M.E.B.), No. R01-EB000419 (M.E.B.), No. R01 AR46996 (M.E.B.), No. R01-HL55686 (M.E.B.), and No. R01-EB002638 (M.E.B.).

APPENDIX A

The following is the general classical derivation for the chirping envelope and frequency variation induced by reference arm dispersion [Eq. (2)]. The phase variation used, when introduced, is a linear phase ramp for convenience. However, other phase variations lead to the same conclusions. Either field in both arms can be expressed as

$$E_R(z) = \frac{1}{2}\int_{-\infty}^{\infty} p_R a_0(k)\exp[i\phi_R(k)]\exp(-i2\pi kz)dk, \tag{A1a}$$

$$E_S(z) = \frac{1}{2}\int_{-\infty}^{\infty} p_S a_0(k)\exp[i\phi_S(k)]\exp(-i2\pi kz)dk, \tag{A1b}$$

where, the light field is described as a planar wave and propagates along the z axis, the origin is located at the beam splitter, $a_0(k)$ represents the amplitude spectrum of source, and $\phi_R(k)$ and $\phi_S(k)$ represents its phase spectrum in the reference arm and sample arm, respectively. The coefficients p_R and p_S are defined as amplitude attenuation in the reference and sample arm, respectively. The phase items in the above can be extended in the second-order Taylor series

$$E_R(z) = \frac{1}{2}\int_{-\infty}^{\infty} p_R a_0(k)\exp\left\{i\left[\phi_R(k_0) + \phi_R'(k_0)(k-k_0) + \frac{1}{2}\phi_R''(k)(k-k_0)^2\right]\exp(-i2\pi kz)dk\right\},$$

$$E_S(z) = \frac{1}{2}\int_{-\infty}^{\infty} p_S a_0(k)\exp\left\{i\left[\phi_S(k_0) + \phi_S'(k_0)(k-k_0) + \frac{1}{2}\phi_S''(k)\times(k-k_0)^2\right]\exp(-i2\pi kz)dk\right\}. \tag{A2}$$

If the dispersion is only introduced in the reference arm, classically group velocity dispersion (GVD) in the sample arm is negligible under these experimental conditions. In other words, the second-order derivative of the phase in the sample arm equals zero. Thus,

$$\phi_R(k_0) = 2\pi n(k_0)k_0 z_R + \phi_0,$$

$$\phi_S(k_0) = 2\pi n(k_0)k_0 z_S + \phi_0, \tag{A3}$$

$$\phi_R'(k_0) = 2\pi[n'(k_0)k_0 + n(k_0)]z_R = 2\pi n_g(k_0)z_R,$$

$$\phi_S'(k_0) = 2\pi[n'(k_0)k_0 + n(k_0)]z_S = 2\pi n_g(k_0)z_S, \tag{A4}$$

$$\phi_R''(k_0) = 2\pi[n''(k_0)k_0 + 2n'(k_0)]z_R,$$

$$\phi_S''(k_0) = 0, \tag{A5}$$

where $n(k)$ represents the refractive index, $n_g(k)$ is the group index, and z_R and z_S represent the path length in the reference arm and the sample arm, respectively. This is in contrast to the nonclassical results found in the text where the refractive index can be a superposition of the medum and the glass slide. Furthermore, we define

$$\frac{\phi_R(k_0) - \phi_S(k_0)}{2\pi k_0} = n(k_0)\Delta z,$$

$$\frac{\phi_R'(k_0) - \phi_S'(k_0)}{2\pi} = n_g(k_0)\Delta z,$$

$$\frac{\phi_R''(k_0) - \phi_S''(k_0)}{2} = 2\pi n'(k_0)z_R + \pi[n''(k_0)k_0]z_R. \tag{A6}$$

The interference signal produced by a single interface is represented as

$$I(\Delta z) = I_R + I_S + 2\,\mathrm{Re}[\Gamma_{RS}(\Delta z)], \tag{A7}$$

where I_R and I_S are the light intensity in the reference arm and the sample arm, respectively, and specifically the correlation function of the reference beam and the sample beam is represented as

$$\Gamma_{RS} = \langle E_R(z)E_S^*(z-\Delta z)\rangle = \frac{1}{4}p_R p_S\int_{-\infty}^{\infty} a_0^2(k)\exp\left(i\left\{[\phi_R(k_0) - \phi_S(k_0)] + [\phi_R'(k_0) - \phi_S'(k_0)](k-k_0) + \frac{1}{2}[\phi_R''(k_0) - \phi_S''(k_0)](k-k_0)^2\right\}\right) \times\exp(-i2\pi k\Delta z)dk, \tag{A8}$$

$$\Gamma_{RS} = \langle E_R(z)E_S^*(z-\Delta z)\rangle = \frac{1}{4}p_R p_S\int_{-\infty}^{\infty} a_0^2(k)\exp\{i[2\pi n(k_0)k_0\Delta z + 2\pi n_g(k_0)\Delta z \times(k-k_0) + 2\pi n'(k_0)z_R(k-k_0)^2 + \pi n''(k_0)z_R(k-k_0)^2]\}\exp[-i2\pi(k-k_0)\Delta z]dk \tag{A9a}$$

$$= \frac{1}{4}p_R p_S\int_{-\infty}^{\infty} a_0^2(k)\exp\{i[2\pi n(k_0)k_0\Delta z + 2\pi n'(k_0)z_R(k - k_0)^2 + \pi n''(k_0)z_R(k-k_0)^2]\}\exp\{i2\pi[n_g(k_0) - 1] \times(k-k_0)\Delta z\}dk, \quad \Delta z = z_R - z_S. \tag{A9b}$$

Thus, $I(\Delta z)=I_R+I_S+2\,\mathrm{Re}[\Gamma_{RS}(\Delta z)]$ could have the following approximation:

$$I(\Delta z) \approx I_R + I_S + \frac{I_0}{2} p_R p_S \cos[2\pi n(k_0) k_0 \Delta z + C] \times \exp\left[- \frac{4 \ln 2 n^2(k_0) \Delta z^2}{\delta_l'^2} \right], \quad \text{(A10)}$$

where δ_l' represents the FWHM width of the envelope in dispersion [expanded by $\pi n''(k_0) z_R$], where δ_l represents nondispersion. Constant C is determined by the dispersion in either arm and contains $2\pi n'(k_0) z_R$.

APPENDIX B

The principles behind the removal of second-order correlations are described here in quantum-mechanical terms. The absorption (detection) electric-field operator for a Gaussian field is given by

$$\hat{E}^{(-)}(r,t) = -id\left(\frac{h\omega}{2\varepsilon_0 V}\right)^{1/2} \times \hat{e}(\hat{a}_1^\dagger + \hat{a}_2^\dagger) e^{i(k\cdot r - \omega t)} e^{-[(r-r_0)^2/2\sigma^2]} \cos(\theta + \phi).$$

All terms are described in the text except V, which represents the volume, e, which is the polarization operator, θ, which defines the carrier frequency, and ϕ, which is a phase shift used in the dual-balanced detection. The intensity is given by

$$I = d^2\left(\frac{h\omega}{2\varepsilon_0 V}\right) \hat{e}^2 (\hat{a}_1^\dagger + \hat{a}_2^\dagger)^2 e^{-[(r-r_0)^2/\sigma^2]} \cos^2(\theta + \phi) = \frac{d^2}{2}\left(\frac{h\omega}{2\varepsilon_0 V}\right) \hat{e}^2 (\hat{a}_1^\dagger + \hat{a}_2^\dagger)^2 e^{-[(r-r_0)^2/\sigma^2]} [1 + \cos(2\theta + 2\phi)].$$

The major difference between detection of first- and second-order correlations is that at the beam splitter before the detector, the electric field is split for the first-order correlations but for second-order correlations, the intensity fluctuations are split.

First Order

With first-order correlations, with the electric field being split at the beam splitter, a $\pi/2$ phase shift occurs between the two beams. After detection, when subtracted, the current has the following value:

$$\frac{d^2}{2}\left(\frac{h\omega}{2\varepsilon_0 V}\right) \hat{e}^2 (\hat{a}_1^\dagger + \hat{a}_2^\dagger)^2 e^{-[(r-r_0)^2/\sigma^2]} \cos(2\theta + 2\times 0) - \frac{d^2}{2}\left(\frac{h\omega}{2\varepsilon_0 V}\right) \hat{e}^2 (\hat{a}_1^\dagger + \hat{a}_2^\dagger)^2 e^{-[(r-r_0)^2/\sigma^2]} \cos\left(2\theta + 2\times \frac{\pi}{2}\right) = d^2\left(\frac{h\omega}{2\varepsilon_0 V}\right) \hat{e}^2 (\hat{a}_1^\dagger + \hat{a}_2^\dagger)^2 e^{-[(r-r_0)^2/\sigma^2]} \cos(2\theta).$$

Second order

With second-order correlations, intensities are split rather than electric fields at the beam splitter, so that no phase shift results at the beam splitter. The subtraction in the electronics therefore results in a current value of zero.

$$\frac{d^2}{2}\left(\frac{h\omega}{2\varepsilon_0 V}\right) \hat{e}^2 (\hat{a}_1 + \hat{a}_2)^2 e^{-[(r-r_0)^2/\sigma^2]} - \frac{d^2}{2}\left(\frac{h\omega}{2\varepsilon_0 V}\right) \hat{e}^2 (\hat{a}_1 + \hat{a}_2)^2 e^{-[(r-r_0)^2/\sigma^2]} = 0.$$

[1] C. Monroe *et al.*, Science **272**, 1131 (1996).
[2] M. Arndt *et al.*, Nature (London) **401**, 680 (1999).
[3] C. H. van del Wal *et al.*, Science **290**, 773 (2000).
[4] J. W. Eslick, H. N. Pham, C. Radu, and A. Puri, Eur. Phys. J. D **38**, 553 (2006).
[5] W. Marshall *et al.*, Phys. Rev. Lett. **91**, 130401 (2003).
[6] B. Yurke and D. Stoler, Phys. Rev. Lett. **57**, 13 (1986).
[7] S. J. D. Pheonix and P. L. Knight, Ann. Phys. **186**, 381 (1988).
[8] A. Einstein, B. Podolsky, and N. Rosen, Phys. Rev. **47**, 777 (1935).
[9] J. S. Bell, Physics (Long Island City, N.Y.) **1**, 195 (1964).
[10] G. Scarcelli, V. Berardi, and Y. Shih, Phys. Rev. Lett. **96**, 063602 (2006).
[11] B. I. Erkmen and J. H. Shapiro, Phys. Rev. A **77**, 043809 (2008).
[12] T. B. Pittman, Y. H. Shih, D. V. Strekalov, and A. V. Sergienko, Phys. Rev. A **52**, R3429 (1995).
[13] Y. Shih, IEEE J. Sel. Top. Quantum Electron. **9**, 1455 (2003).
[14] D. Bouwmeester *et al.*, Nature (London) **390**, 575 (1997).
[15] L. K. Grover, Phys. Rev. Lett. **79**, 325 (1997).
[16] A. Ekert and R. Jozsa, Rev. Mod. Phys. **68**, 733 (1996).
[17] T. Jennewein, C. Simon, G. Weihs, H. Weinfurter, and A. Zeilinger, Phys. Rev. Lett. **84**, 4729 (2000).
[18] M. H. Rubin, D. N. Klyshko, Y. H. Shih, and A. V. Sergienko, Phys. Rev. A **50**, 5122 (1994).
[19] S. B. Zheng, Phys. Rev. A **75**, 032114 (2007).
[20] J. H. Shapiro and K. X. Sun, J. Opt. Soc. Am. B **11**, 1130 (1994).
[21] K. F. Lee and J. E. Thomas, Phys. Rev. A **69**, 052311 (2004).
[22] M. D'Angelo, A. Valencia, M. H. Rubin, and Y. Shih, Phys. Rev. A **72**, 013810 (2005).
[23] R. S. Bennick, S. J. Bentley, and R. W. Boyd, Phys. Rev. Lett. **89**, 113601 (2002).
[24] A. Valencia, G. Scarcelli, M. D'Angelo, and Y. Shih, Phys. Rev. Lett. **94**, 063601 (2005).
[25] A. Gatti, E. Brambilla, M. Bache, and L. A. Lugiato, Phys. Rev. A **70**, 013802 (2004).
[26] R. Filip, M. Dušek, J. Fiurášek, and L. Mišta, Phys. Rev. A **65**, 043802 (2002).
[27] V. Vedral, M. B. Plenio, M. A. Rippin, and P. L. Knight, Phys.

Rev. Lett. **78**, 2275 (1997).
[28] S. Bose and V. Vedral, Phys. Rev. A **61**, 040101(R) (2000).
[29] S. Bose, I. Fuentes-Guridi, P. L. Knight, and V. Vedral, Phys. Rev. Lett. **87**, 050401 (2001).
[30] A. Furusawa *et al.*, Science **282**, 706 (1998).
[31] C. H. Bennett, G. Brassard, C. Crépeau, R. Jozsa, A. Peres, and W. K. Wootters, Phys. Rev. Lett. **70**, 1895 (1993).
[32] S. Pirandola, D. Vitali, P. Tombesi, and S. Lloyd, Phys. Rev. Lett. **97**, 150403 (2006).
[33] D. Rohrlich, Y. Neiman, Y. Japha, and R. Folman, Phys. Rev. Lett. **96**, 173601 (2006).
[34] J. Zhang, K. Peng, and S. L. Braunstein, Phys. Rev. A **68**, 013808 (2003).
[35] M. E. Brezinski, *Optical Coherence Tomography: Principles and Applications* (Academic, Burlington, MA, 2006).
[36] D. Huang, E. A. Swanson, C. P. Lin, J. S. Schuman *et al.*, Science **254**, 1178 (1991).
[37] M. E. Brezinski, G. J. Tearney, B. E. Bouma, J. A. Izatt, M. R. Hee, E. A. Swanson, J. F. Southern, and J. G. Fujimoto, Circulation **93**, 1206 (1996).
[38] A. G. Podoleanu, Appl. Opt. **39**, 173 (2000).
[39] G. J. Tearney, M. E. Brezinski, B. E. Bouma, S. A. Boppart, C. Pitris, J. F. Southern, and J. G. Fujimoto, Science **276**, 2037-9 (1997).
[40] B. Liu, E. A. Macdonald, D. L. Stamper, and M. E. Brezinski, Phys. Med. Biol. **49**, 923 (2004).
[41] G. J. Tearney, M. E. Brezinski, J. F. Southern, B. E. Bouma, M. R. Hee, and J. G. Fujimoto, Opt. Lett. **20**, 2258 (1995).
[42] W. K. Niblack, J. O. Schenk, B. Liu, and M. E. Brezinski, Appl. Opt. **42**, 4115 (2003).
[43] M. B. Nasr, B. E. A. Saleh, A. V. Sergienko, and M. C. Teich, Phys. Rev. Lett. **91**, 083601 (2003).
[44] M. B. Nasr, B. E. Saleh, A. V. Sergienko, and M. C. Teich, Opt. Express **12**, 1353 (2003).
[45] S. Mancini, V. I. Man'ko, and P. Tombesi, Phys. Rev. A **55**, 3042 (1997).
[46] A. Bassi, E. Ippoliti, and S. L. Adler, Phys. Rev. Lett. **94**, 030401 (2005).
[47] S. Mancini, V. Giovannetti, D. Vitali, and P. Tombesi, Phys. Rev. Lett. **88**, 120401 (2002).
[48] S. Bose, K. Jacobs, and P. L. Knight, Phys. Rev. A **59**, 3204 (1999).
[49] A. Ferreira, A. Guerreiro, and V. Vedral, Phys. Rev. Lett. **96**, 060407 (2006).
[50] D. F. Nelson, Phys. Rev. A **44**, 3985 (1991).
[51] D. Davé and T. Milner, Opt. Lett. **25**, 227, (2000).
[52] D. Dave *et al.*, Opt. Lett. **193**, 39 (2001).
[53] C. K. Hitzenberger and A. F. Fercher, Opt. Lett. **24**, 622 (1999).
[54] N. Linden, S. Popescu, and J. A. Smolin, Phys. Rev. Lett. **97**, 100502 (2006).
[55] K. Wang and D. Z. Cao, Phys. Rev. A **70**, 041801(R) (2004).
[56] M. Fox, *Quantum Mechanics: An Introduction* (Oxford Univeristy Press, 2007).
[57] Z. Ficek and S. Swain, *Quantum Interference and Coherence* (Springer Inc., New York, 2005).
[58] A. Valencia, G. Scarcelli, M. D'Angelo, and Y. Shih, Phys. Rev. Lett. **94**, 063601 (2005).
[59] A. Gatti, E. Brambilla, M. Bache, and L. A. Lugiato, Phys. Rev. A **70**, 013802 (2004).
[60] I. Chang, R. R. Laflamme, P. Shor, and W. Zurek, Science **270**, 1633 (1995).
[61] R. Penrose, Gen. Relativ. Gravit. **28**, 581 (1996).